# Contribution of automatically generated radar altimetry water levels from unsupervised classification to study hydrological connectivity within Amazon floodplains

Pauline Enguehard, Frédéric Frappart, Pierre Zeiger, Fabien Blarel, Frédéric Satgé, Marie-Paule Bonnet

Journal of Hydrology: Regional Studies 47 (2023) 101397

Contents lists available at ScienceDirect

Journal of Hydrology: Regional Studies

journal homepage: www.elsevier.com/locate/ejrh

# Contribution of automatically generated radar altimetry water levels from unsupervised classification to study hydrological connectivity within Amazon floodplains

Pauline Enguehard [a,*], Frédéric Frappart [b,c], Pierre Zeiger [c], Fabien Blarel [b], Frédéric Satgé [a], Marie-Paule Bonnet [a]

[a] ESPACE-DEV, IRD, University of Montpellier, 34093 Montpellier, France
[b] INRAE, Bordeaux Sciences Agro, UMR 1391 ISPA, 33140 Villenave-d'Ornon, France
[c] LEGOS, CNRS/CNES/IRD/UPS, 31400 Toulouse, France

ARTICLE INFO

*Keywords:*
Radar altimetry
Amazon
Floodplains
Unsupervised classification
Automatic generation of water level gauges
Hydrological connectivity

ABSTRACT

*Study region:* The Curuaí floodplain in the low Amazon river in the Pará state of Brazil and Juruá basin, a major Solimões tributary.
*Study focus:* Characterizing the hydrological dynamics of Amazon floodplains is essential to better understand and preserve these environments providing important resources to local populations. Radar altimetry is an effective remote sensing tool for monitoring water levels of continental hydrosystems, including floodplains. An unsupervised classification approach on radar echoes to determine hydrological regimes has recently been tested and showed a strong potential on the Congo River basin. This method is adapted to Envisat and Saral satellite radar altimetry data on two study areas in the Amazon Basin. The aim is to improve inland water detection along altimeter tracks to automatically generate water level time series (WLTS) over rivers, lakes, and poorly monitored floodplains and wetlands.
*New hydrological insights:* Results show a good agreement with land cover maps obtained with optical imagery over selected Amazonian wetlands (70–80% accuracies with Envisat data and 50–60% with Saral data). Automatically generated WLTS are strongly correlated to the manually generated WLTS ($R^2 \approx 0.9$; RMSE $< 1$ m). Compared to the manual method, the automatic method is faster, more efficient and replicable. Densifying the WL network in the floodplains bring crucial information on the connectivity dynamic between lakes and rivers.

## 1. Introduction

Freshwater wetlands and floodplains cover ~8% of the Earth's surface (Davidson et al., 2018). They have an essential role in fluvial hydrological dynamic regulation, organic and inorganic dissolved and particulate material fate, and water quality (Costanza et al., 1997; Jisha and Puthur, 2021; Xu et al., 2019). It also ensures fundamental functions such as flood mitigation, groundwater recharge, water purification, nutrient and sediment retention, and supports high levels of biodiversity (Dudgeon et al., 2006). Today, wetland ecosystems are well documented (Davidson et al., 2018; Janse et al., 2019; Jisha and Puthur, 2021) and turn out to be the most

* Corresponding author.
*E-mail address:* pauline.enguehard@ird.fr (P. Enguehard).

https://doi.org/10.1016/j.ejrh.2023.101397

Available online 27 April 2023

threatened ecosystems ("Media Release: Nature's Dangerous Decline 'Unprecedented'; Species Extinction Rates 'Accelerating' | IPBES secretariat," 2019; Moomaw et al., 2018) requiring the most effective preservation (Dubos et al., 2022). Sixty-six percent of the continental biodiversity extinctions are aquatic taxa and habitat's loss rate is greater than biodiversity extinctions (Denny, 1994; Foley et al., 2007). Amazon is the largest river system in the world, with about 6,400,000 km$^2$ and the largest freshwater reserve concentrates 16% of the planet's freshwater flow (da Silva Abel et al., 2021; Latrubesse et al., 2017). Wetlands and floodplains in this watershed represent 800,000 km$^2$, which is about 10% of the total basin area (Melack and Hess, 2010). Hydrological cycle of the main river and in these areas is considered as a key factor in regulating biodiversity (Junk et al., 2014, 1989). Indeed, wetlands are a major biodiversity

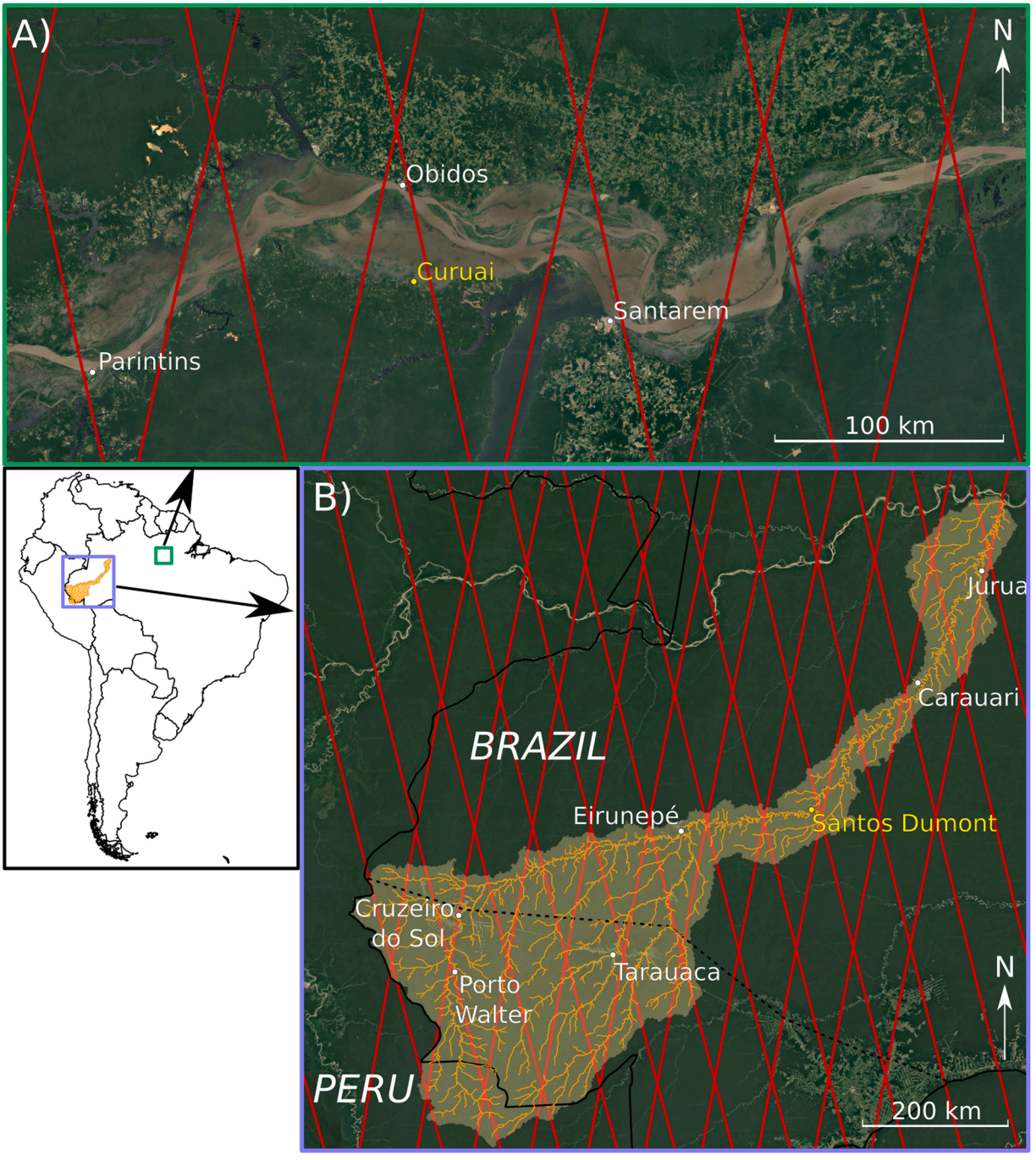


**Fig. 1.** – A) Curuaí floodplain on the right margin of the Amazon River. B) Juruá watershed and its water drainage network. The radar altimeter tracks of Envisat and Saral missions, that had the same orbit, appear in red. Water level gauges used as references in this study are shown in yellow. (Background maps: Google Earth, HYDROSHEDS).

reserve, regulating many species life cycle of fauna and flora and hosting characteristic biotopes (da Silva et al., 2013; Jézéquel et al., 2020). For example, in the whitewater rivers of the Amazon, fish communities vary markedly and predictably with hydrological season. Their reproduction is synchronized with the onset of the rainy season (da Silva et al., 2013) when the hydrological connectivity through surface water is maximum. Indeed, each year the seasonal flood leads to an important rise of the WL in the river, which invades the vast associated floodplains and increases the connectivity among rivers, lakes and wetlands, resulting in an intensification of nutrients and organisms exchange required for fish life cycles (da Silva et al., 2013; Trigg et al., 2012). Furthermore, because of their relative accessibility, soil fertility and fishy water, floodplains are heavily populated areas in the Amazon. Economic activities in these areas are directly influenced by climate and river water dynamics that control development of productive activities (agriculture, fishing, logging) (Sousa and Oliveira, 2016). Nevertheless, climate change and deforestation, leading to more frequent and severe droughts and floods (Marengo and Espinoza, 2016), and anthropic activities, such as hydroelectricity production, mining and urban occupation along banks of rivers, are all threats to these systems, their biodiversity and related economic activities (Melack et al., 2021). In this context, the characterization of the hydrological connectivity is a key issue to better interpret biogeochemical cycles or fish population dynamics, for example (Park and Latrubesse, 2017).

Nowadays, most of the *in situ* water level (WL) stations in the world are located on river main courses or on largest lakes. Since the beginning of the 2000 s, Vorosmarty et al. (2001) have been concerned about the decreasing number of *in situ* stations, which is partly related to the maintenance costs of the networks. The Amazonian *in situ* network has only gauges located in the rivers, except Curuaí gauge which is the only one acquiring water level in a floodplain. The development of alternative observation systems for *in situ* networks are thus necessary to improve our ability to monitor the wetlands' possible evolution in response to the above cited threats (climate change, dam). In this regard, remote sensing techniques offer a unique opportunity to monitor large watersheds' hydrology and characterizing connectivity in areas where *in situ* information is lacking because of difficult access, as it is the case for Amazon wetlands (Alsdorf et al., 2007, 2000; Jung et al., 2010; Park, 2020). Advantages of satellite systems are widely known: almost global coverage, spatial and temporal consistency of data, archiving of past data, durability and continuity of data are guaranteed (Fassoni-Andrade et al., 2020; Rast et al., 2014). Surface water monitoring requires the mapping of the flooded areas and information on their WL to determine the water storage (Alsdorf et al., 2001; Arnesen et al., 2013; Papa and Frappart, 2021). In order to determine wetlands extent, radar sensors have strong advantages compared to optical ones as they provide information on land surfaces in all weather conditions, during day or night times. Moreover, lower frequencies electromagnetic waves in the microwave domain (*e.g.* L-band) can penetrate through the vegetation cover which can be very dense in the Amazon (Hess, 2003; Frappart et al., 2015; Shu et al., 2021), especially radar altimeters and their nadir-pointing vision (mostly operating at Ku or Ka frequency bands). These characteristics allow altimeters to measure land surfaces information (*e.g.* distance between the satellite and the reflecting surface, backscattering coefficient; Frappart et al., 2006; Frappart et al., 2021b) and thus obtain surface WL. This technique has been widely used over the past two decades to monitor the temporal variations of WL of lakes and rivers (Abdalla et al., 2021). However, few studies used radar altimetry data to monitor floodplain WLs (see Papa and Frappart in, 2021 for a review), whereas this is a considerable information source.

This study aims to classify altimeter radar echoes in water-covered classes and create WL time series for each representative groups over Amazon floodplains. As WL time series in these areas are non-existent for now, their creation could considerably densify the WL station network in the Amazon. For this purpose, we follow a method based on an unsupervised classification of radar echoes to distinguish different hydrological regimes which automatically generate WL time series along altimeter tracks over the rivers and the floodplains (applied on the Congo river basin in Africa (Frappart et al., 2021c). This method is applied and adapted to two study areas in the Amazon to test the method replicability in the most tropical-wooded areas and densify the non-existent WL network in floodplains. Indeed, this study targets study areas where floodplains are playing a key role for biodiversity and local populations.

## 2. Materials

### 2.1. Study area

The study areas are composed of floodplains located in two major whitewater rivers (Fig. 1): the Amazon River in the surroundings of Óbidos (Pará) (from 1.63° to 2.75° S; from 53.27° to 56.80° W) and one of the Solimões tributaries, the Juruá (from 2.45° to 8° S; from 65.75° to 73° W). The Lago Grande de Curuaí floodplain (referred as Curuaí floodplain, hereafter) is separated from the Amazon mainstream to the north by narrow levees and to the south by upland (terra firme). It is composed of several large and shallow lakes connected temporary or permanently to the mainstream by several channels. The flooded area can vary from less than 600 $km^2$ up to 2500 $km^2$ during floods, with the maximum flood flow having a return period between 5 and 10 years (Bonnet et al., 2008; Callede et al., 2002). Each year, the rising phase of the floodplain starts between November and December and reaches its maximum in May-June. The falling phase begins in July and lasts until November with the greatest volume exported occurring from August to September. The climate of the Curuaí várzea is tropical monsoon with a mean annual temperature of about 26.5 °C and a mean annual rainfall of 2033 mm (Bonnet et al., 2008).

Climate in Juruá basin is very similar, with also two distinct seasons: the dry season, which extends from April to September, and the rainy season, which extends from October to March (da Silva Abel et al., 2021). Annual rainfall generally ranges between 1800 and 2200 mm and average annual temperature is about 24.5 °C. The Juruá basin is one of the most important basins in the southwestern Amazon, with a territorial extension of 224,000 $km^2$. Its source is at an altitude of about 453 m in the Ucayali region of Peru (10.05° S, 72.49° W; (Sousa and Oliveira, 2016). The river course extends over 3280 km, until it reaches its mouth in the northeast, joining the right bank of the Solimões River at an altitude of 36 m (2.63° S, 65.76° W). Over its entire course, the river has a difference in altitude of more than 400 m, giving a slope of about 0.007°/km. According to the fluvial morphology, the Juruá is classified as a meandering

river with high sinuosity, high-suspended load and relative stability (Mota Da Silva, 2020). It is considered the most meandering river in the world, characterized by numerous irregular and tortuous meanders, with a huge floodplain of over 20,400 km$^2$ containing thousands of lakes, many of which are abandoned meanders (Sousa and Oliveira, 2016).

### 2.2. Datasets

#### 2.2.1. Altimetry datasets

Radar altimetry data used in this study were acquired by Envisat and Saral on their nominal orbits. They were placed on a ~790 km sun-synchronous orbit with a 98.54° inclination sun-synchronous orbit with a 35-day repeat cycle and an equatorial ground-track spacing of about 85 km. Envisat payload was composed of 10 instruments including the advanced radar altimeter (RA-2). RA-2 was a nadir-looking pulse-limited RA operating at two frequencies: Ku- (~13.575 GHz) and S-(~3.2 GHz) bands (Benveniste et al., 2003). Data were acquired from 05/2002–10/2010. The radar footprint is ~15 km diameter which leads to more than 200 km$^2$ of coverage. Ku-band measurements are acquired with ~350 m space between footprints along the satellite tracks. Saral payload was composed of 4 instruments including the altimeter radar AltiKa, which is the first altimeter to operate at Ka-band (~35.5 GHz; (Verron et al., 2015). Data were acquired from 02/2013–07/2016. The radar footprint is 8 km diameter which leads to more than 60 km$^2$ of coverage. Higher pulse repeat frequency (500 MHz against 320 MHz) of Saral allows a shorter space of ~180 m between footprints along the satellite tracks. Saral has a smaller footprint and higher along-track and vertical resolutions than Envisat (Bonnefond et al., 2018; Verron et al., 2021).

Radar altimeter measures the two-way travel time of the electromagnetic pulse emitted by the sensor and the power reflected by the Earth's surface. The two-way travel-time is used to derive an approximate distance between the satellite and the surface. The analysis of the radar echo (power received by the satellite as a function of the time) allows to refine the distance estimate applying a retracking process and to estimate the backscattering coefficient (Cretaux et al., 2017). Two types of altimetry data are used here: raw data from the Geophysical Data Records (GDR) and normalized tracks data. These are computed along each ground-track clustering and for each cycle to obtain 3D gridded information (see Frappart et al., 2021c for more details). Both datasets are made available by the CTOH through AlTiS data request from http://ctoh.legos.obs-mip.fr.

#### 2.2.2. Reference land cover map

The reference land cover map will be used as validation of the radar echoes classifications, by constructing confusion matrices (Section 4.1.1). The Curuaí region map is from (Arantes et al., 2019); Supplementary Material Figure A.A). The Juruá basin's map is

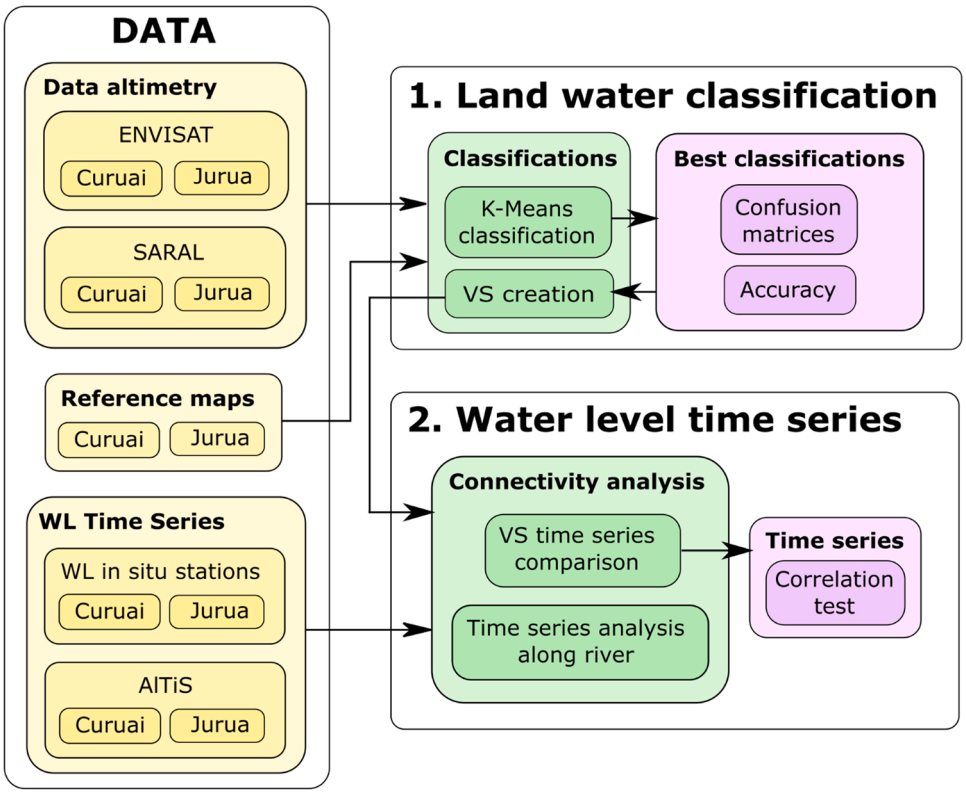


**Fig. 2.** – Flow chart of the approach applied in this study.

shown in Supplementary Material Figure A.B and is available on ORNL DAAC for Biogeochemical Dynamics website (http://daac.ornl.gov). High water season maps is available and used here to see the entire inundation extent. The overall accuracy for wetland mapping is 93% and 86% for vegetation mapping (Hess et al., 2015). Curuaí and Juruá regions' morphologies and properties are totally contrasted in terms of vegetation density and river width which allow us to test the method in different environments.

#### 2.2.3. Water level time series

*2.2.3.1. WL gauge stations.* WL gauge records are used to validate the automatically-generated WL from radar altimetry. Data was downloaded from the water's Brazilian national agency website Hidro-Telemetria (http://www.snirh.gov.br/hidrotelemetria/Mapa.aspx). One WL gauge located in the Lago Grande (2.25° S, 55.33° W), near Curuaí , has collected data since 1982 and has been levelled by high precision GPS based on WGS84 coordinate system (Calmant et al., 2013) and reported to EGM2008 gravity field model (Pavlis et al., 2012). In the Juruá watershed, the Santos Dumont WL gauge (6.44° S, 68.24° W) is chosen to be the reference because of its proximity to a satellite track and its similar WL recording's period. This WL gauge is about 3000 km upstream from the mouth of the Juruá (see Fig. 1) and record WL since 1981. It has not been levelled, the comparison with altimetry data will be in a relative way to focus on the hydrological cycle's changes.

*2.2.3.2. AlTiS time series.* Time series of WL can be manually retrieved using the Altimetry Time Series (AlTiS) software (Frappart et al., 2021a), a new version of the MAPS software (Multi-mission Altimetry Processing Software; (Frappart et al., 2015b; Normandin et al., 2018). These time series of WL are used to validate the automatic method presented in this study. The software enables the user to select the altimetry data inside a Google Earth polygon. It can display parameters supplied by CTOH: backscatter coefficients and WL estimations. These parameters are presented as time series obtained computing the median of each cycle valid observations following the processing proposed in Cretaux et al. (2017). Some outliers may still be present in the time series and can be manually removed thanks to a specialized tool.

## 3. Methods

### 3.1. Methodology summary

The method applied in this study to generate WL from a classification of the radar altimetry echoes is summarized in Fig. 2. First step consists of applying a K-means unsupervised classification technique to radar altimetry parameters as in Frappart et al. (2021c). Then, best parameter combinations are determined with confusion matrices and accuracy computing. Finally, VS were built on the water-covered surfaces and some comparisons are presented, with *in-situ* and AlTiS software.

### 3.2. Classification of radar altimetry echoes

#### 3.2.1. Temporal variations of radar altimetry data

The classification's methodology is applied to one or several radar altimetry parameters as their responses differ according to the presence or not of water. Over open water areas such as rivers and lakes, there are large seasonal variations in the backscatter coefficient in Ku- and Ka-bands (Supplementary Material Figure B; Frappart et al., 2021a, 2021b). These temporal variations are related to changes in river width or lake extent in the altimeter footprint, caused by the increase in WL. The larger the water extent, the more power backscattered to the radar altimeter as this sensor is nadir-pointing. Large variations of the backscatter coefficients occur along the hydrological cycle, well-synchronized with the temporal variations of the WL over rivers and lakes. In the Amazon, maxima occur in May/June and minima in November/December. There is smaller variation in the backscatter coefficient over the flooding forests, but some variation still remains due to changes in flooding extent present in the several km-wide altimeter footprints. Even when the

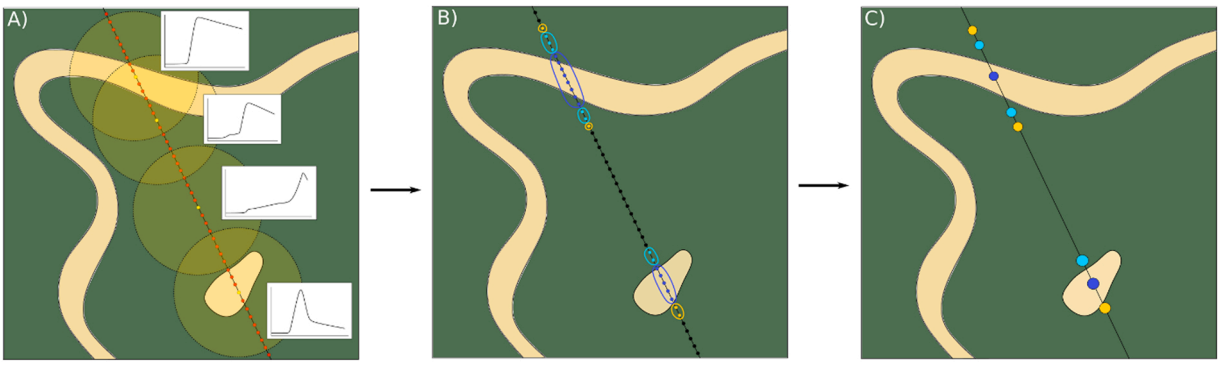


**Fig. 3.** – (A) Radar altimetry echoes are different regarding the radar footprint. (B) Radar altimetry echoes are classified in function of the echoes' shapes and (C) for each class, a VS is created.

flooded areas are under vegetation, large backscattering responses are observed (Frappart et al., 2015a; Frappart et al., 2021b), and time series of water levels can be derived (Frappart et al., 2006; Frappart et al., 2021c). Over non-flooded forest, smaller variations of backscattering and height are observed, not related to the changes caused by the hydrological cycle (see also Frappart et al., 2015b; Frappart et al., 2021a). These changes can be mostly attributed to orbital drifts (plus or minus 1 km around the nominal orbit of the satellite) and to changes in local roughness as the wavelength of the electromagnetic waves at Ku- and Ka-bands is lower than 0.1 m. The chaotic variations in the height observed in the Envisat and Saral time series are outliers. When the tracking is operating well, the height is estimated to be continuous.

These very different temporal behaviors, observed in radar altimetry echoes over open water and forest-covered areas, are used to classify the echoes by type of aquatic environment. The unsupervised clustering algorithm K-means is used in our method to classify echoes (Jain and Dubes, 1988; Likas et al., 2003). K-means is suitable for our purpose as no training dataset can be used due to the complexity of the radar altimeter echoes in very heterogenous environments (Stammer and Cazenave, 2017). Echoes are grouped into K different clusters, based on their shape similarities (see Fig. 3. A), translating the soils backscatter coefficient and, thus, characterizing the land cover. A Python algorithm is used to obtain these K groups and classify them as Fig. 3 show it (panel B), and process to VS creation (panel C).

#### 3.2.2. Echoes classifications

Tests were conducted considering three to six classes. By taking into account the classification test results and as an analysis of the best number of classes was already performed in a previous study (Frappart et al., 2021c), the optimal number of K classes is four (0−3) to best represent the different hydrological regimes in the Amazon rivers, lakes and wetlands, without over-interpreting the radar echoes (Kodinariya and Makwana, 2013). However, Curuaí and Juruá's classes of the validation maps are more than four. In order to simplify the comparison, closest aquatic environments were grouped together to approximate our four classes classification to assess. Table 1 summarizes the validation groups of reference classes for our radar echo classification.

The radar altimetry echoes are classified according to three combinations of parameters: backscatter coefficient only (B) (as in Frappart et al., 2021c), backscatter coefficient and raw WL (B+RWL), and backscatter coefficient and normalized WL (B+NWL). Indeed, the backscatter coefficient is an important parameter to keep to detect the water presence and WL normalization highlights major phases of the hydrological regime, in contrast to raw WL, where the amplitude variations are highlighted.

#### 3.2.3. Classification validation

Then, the best parameter accuracy combination is determined for each satellite mission over each study area by analysing confusion matrices between reference land cover maps (see Fig. Annexe A) and our classifications. Confusion matrices and accuracies are calculated to quantify the agreement between both and determine the best combination of parameters. For each confusion matrix obtained with the classifications, the accuracy index is calculated (Eq. 1). This index determines which combination of parameters gives the best classification of radar altimeter echoes. It can take values ranging from 0 for poor accuracy, to 1 for very good accuracy.

$$(TP + TN) / (TP + FP + TN + FN) \quad (1)$$

With TP = True Positive, FP = False positive, TN = True negative and FN = False negative.

### 3.3. WL Time series

#### 3.3.1. Automatic generation of WL time series

Time series of altimetry-derived water levels are generated over the clusters identified as covered with water (*i.e.*, open water and flooded areas). For each water-covered classes (0−2), a virtual station (VS) is created (Fig. 3. C), indicating the intersection between the ground and a water body. VS are created under some conditions depending on water bodies widths:

- A minimal number of 5 radar echoes is required for creating a VS in Curuaí . For Juruá watershed, the minimal number is 1 because of the narrowness of the river sections where variations in surface type can be spatially significant.

**Table 1 –**
List of the Curuaí and Juruá's reference map classes grouped for the validation of the radar echo classification.

| Curuaí (Arantes et al., 2019) | |
|---|---|
| Classification group | Reference map classes |
| Open water | Mainstem channel + Lakes and channels |
| Semi-permanent inundation | Grassland habitat exposed only at very low water |
| Intermediate inundation | Grassland habitat exposed at mid water |
| High level inundation | Grassland habitat exposed only at high water |
| Non-inundated | Forest + Shrub + Urban + Outside study area |
| Juruá (Hess et al., 2015) | |
| Open water | Open water + Aquatic macrophyte |
| Flooded | Flooded shrub + Flooded woodland + Flooded forest |
| Non-flooded | Non-wetland + Non-flooded forest |

- The distance between two radar echoes from the same VS of one class must be less than 5 km in Curuaí / 1.5 km in the Juruá watershed.
- The distance between two VS from any class must be at least 1 km in Curuaí and in the Juruá watershed.
- The maximal distance for a VS' process from the same class is 50 km in Curuaí / 5 km in the Juruá watershed.

Then, a WL time series is automatically created for each VS. To be sure of the classification parameter to keep for WL time series study, VS are numerically analysed. These results are presented in sub-Section 4.1.

### 3.3.2. *WL time series validation*

In order to validate the automatic method, time series from the parameter presenting the best classification accuracies is analysed here. Curuaí and Juruá's time series of WL are compared with the manually retrieved time series of WL obtained using the AlTiS software and to *in situ* data. These time series are compared in terms of anomalies of WL. Validation between created VS from the three water-presence classes with the *in situ* data and AlTiS software-based WL are achieved by correlation test of $R^2$ and RMSE. Some WL comparison results are shown in Section 4.2.

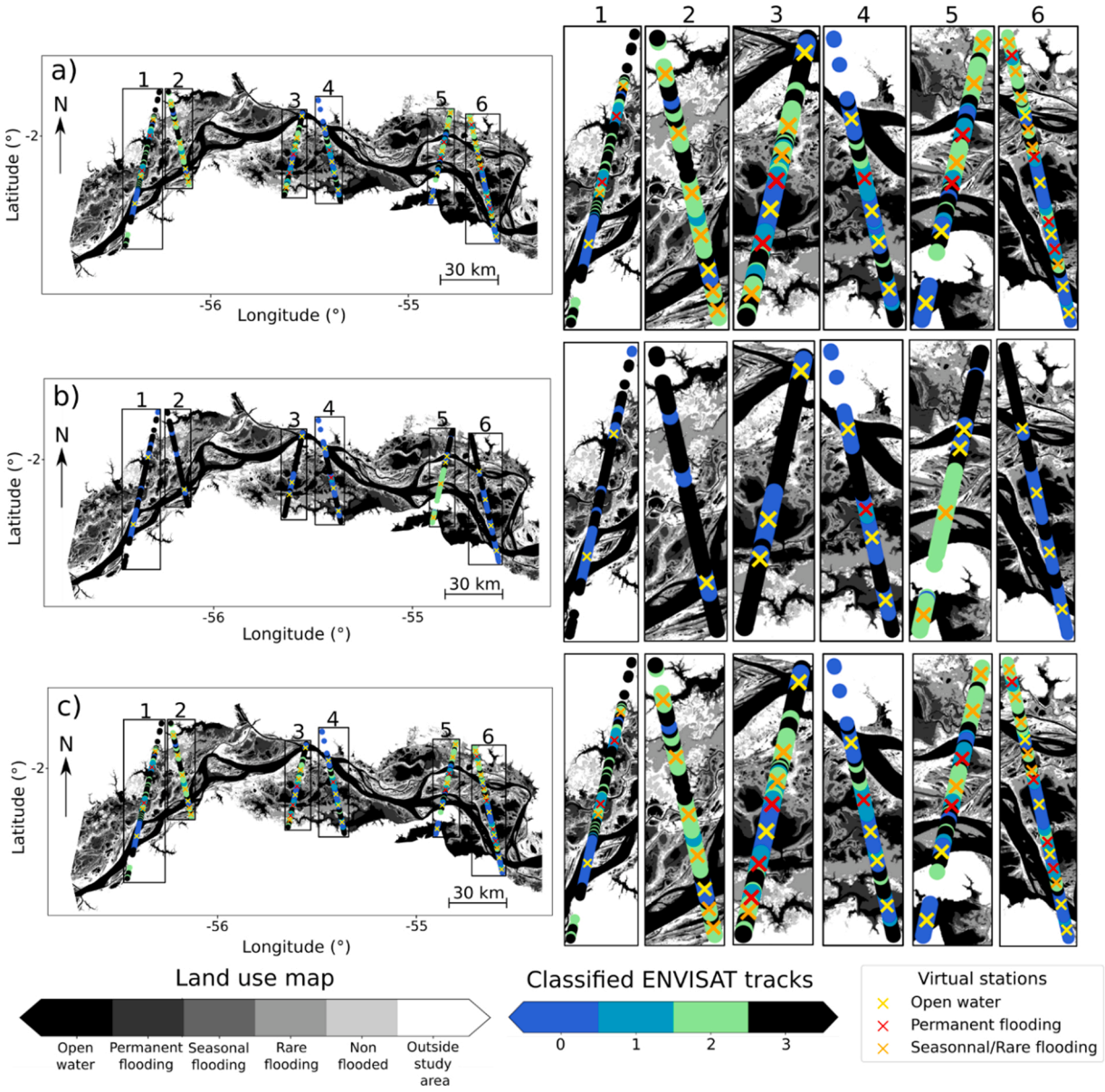


**Fig. 4.** – K-Means classifications of the Envisat radar echoes over Curuaí according to (a) the backscatter coefficient only, (b) the backscatter coefficient and raw WL and (c) the backscatter coefficient and normalized WL.

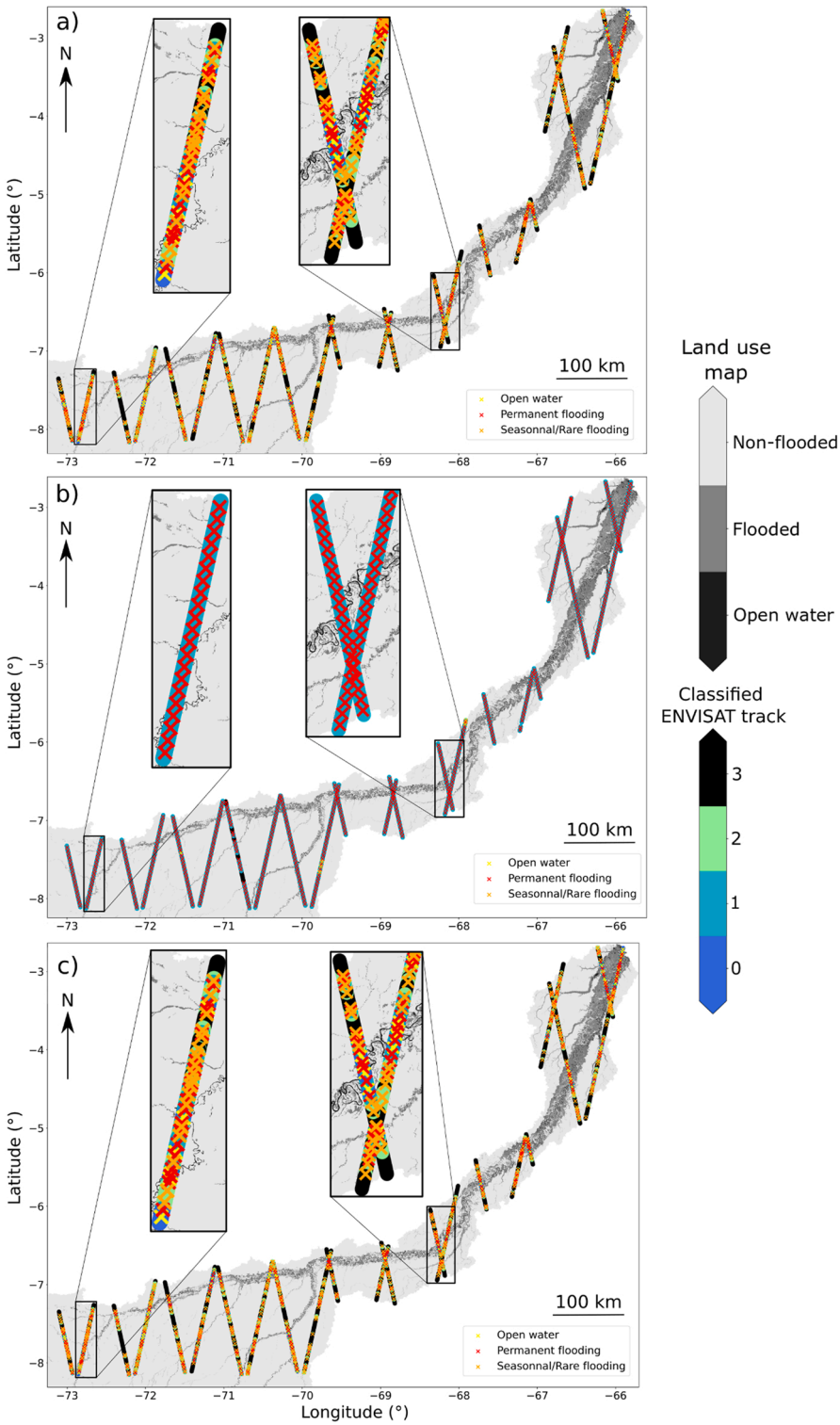


**Fig. 5.** – K-Means classifications of the Envisat radar echoes over Juruá according to (a) the backscatter coefficient only, (b) the backscatter coefficient and raw WL and (c) the backscatter coefficient and normalized WL.

## 4. Results

### 4.1. Radar echoes classification and virtual station detection

#### 4.1.1. Classification of radar altimetry echoes

The results of the along-track classifications of Envisat and Saral radar echoes over Curuaí and the Juruá river are shown in Figs. 4, 5 and Supplementary Material Figures C and D, respectively, for each parameter. Corresponding confusion matrix results computed between reference class maps and radar echoes classifications are shown in Fig. 6, more details are presented in Supplementary Material Tables A and B. The four classes represent all the major hydrological regimes present in the study areas. Very similar results were obtained when considering four to six classes (as in Frappart et al., 2021c not shown here) but best solutions were obtained with four classes. Classes 0 and 3 represent the most and the least widely covered with water areas, respectively. Classes 1 and 2 correspond to intermediate water regimes, class 1 corresponding with longer presence of water than class 2. For Envisat results over Curuaí region, true positive (TP) and false negative (FN) results are predominant (70–80%), representing good correlation, for both parameters with a slightly better class correlation for B+NWL parameter. Concerning Saral results over Curuaí , 60% of the results are in good agreement with the map references for B and B+NWL parameters, but only 25% are in good agreement for B+RWL parameter. For Envisat results over the Juruá watershed, 41% of the B and B+NWL results and 25% of the B+RWL results are in good agreement with map reference classes. Concerning Saral results over Juruá watershed, 33% of the B and B+NWL results and 25% of the B+RWL are in good agreement.

#### 4.1.2. Classification selection

Classification accuracies are shown in Table 2. Accuracy varies between 0.52 and 0.74 for B and B+NWL parameters and between 0.25 and 0.59 for B+RWL parameter. Indeed, mixing effects between different types of soil due to the large radar footprint over the surface are taken into account, which can explain the moderate accuracy values. Considering the very small differences between B and B+NWL accuracies, we only focus on the B+NWL parameter because of its innovative character. These results are available online on the data repository (Enguehard et al., 2023).

#### 4.1.3. Virtual station creation

For each series of radar echo in the same class and respecting the conditions listed in Section 3.3, a VS is created. Fig. 7 presents the number of VS created according to the different combination of parameters and area/satellite (independently from the accuracies). First, we can see that the B+RWL combination does not allow to create more than 10 VS for at least two classes, except for the Juruá/Saral combination where class 0 is over-represented (more than 500 VS). In contrast, B and B+NWL present similar distribution for

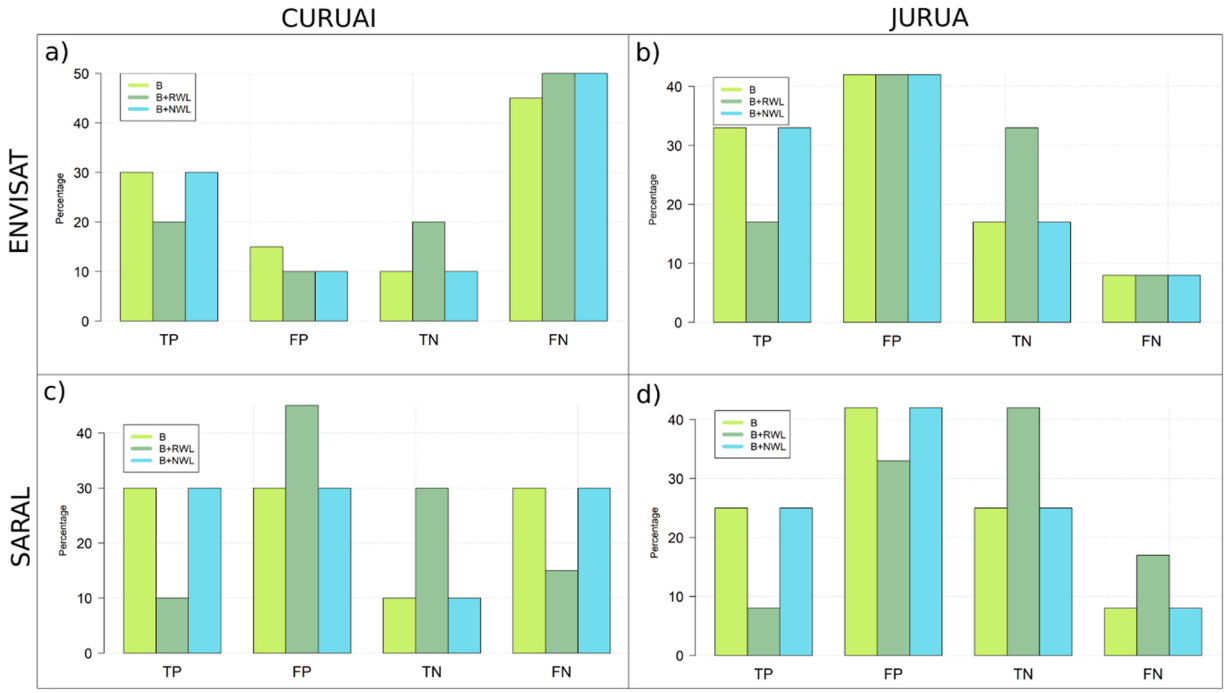


**Fig. 6.** – Confusion matrix results for (a) Curuaí Envisat classification, (b) Juruá Envisat classification, (c) Curuaí Saral classification and (d) Juruá Saral classification for each parameter results: backscatter only (B), backscatter and raw WL (B+RWL) and backscatter and normalized WL (B+NWL). TP = True Positive, FP = False positive, TN = True negative and FN = False negative.

**Table 2**
Classification accuracies over Curuaí and Juruá watershed with Envisat and Saral data for both three parameters.

| | B | B+RWL | B+NWL |
|---|---|---|---|
| Curuaí / Envisat | 0.740 | 0.592 | 0.741 |
| Curuaí / Saral | 0.525 | 0.422 | 0.525 |
| Juruá / Envisat | 0.685 | 0.510 | 0.685 |
| Juruá / Saral | 0.592 | 0.252 | 0.594 |

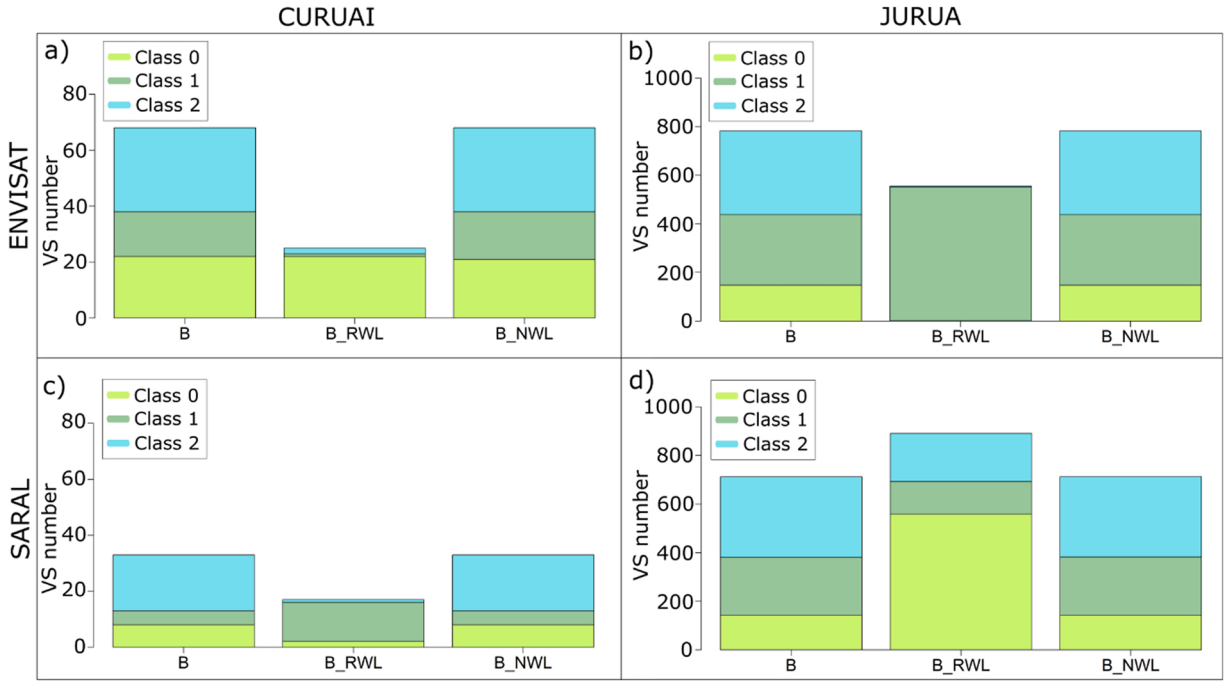


**Fig. 7.** – Number of VS created with Envisat over (a) Curuaí and (b) the Juruá and with Saral over (c) Curuaí and (d) the Juruá.

each area/satellite combination. As expected, there is much more class 1 VS created in the Juruá than in Curuaí because of the largest floodplain area crossed by the altimeter. Finally, Envisat and Saral exhibit similar VS classes distributions in Juruá and Curuaí for B and B+NWL parameters but much less VS are created for Curuaí /Saral compared to Curuaí /Envisat, probably due to the only 3 years of Saral data used here compared to the 8 years of Envisat data. However, the method proves to be efficient to create VS over Amazon floodplains.

### *4.2. WL time series validation*

Time series of WL results are available online on the data repository (Enguehard et al., 2023). Here, we choose to focus on B+NWL time series because of its innovative character compared to the B parameter that has been already studied (Frappart et al., 2021c). With the large number of results, only VS at the closest location to the gauging stations have been selected for comparison. Figs. 8 and 9 present these VS, as well as the $R^2$ and RMSE between our results and those obtained using AlTiS software. Supplementary Material Figs. E and F are presenting $R^2$ and RMSE between our results/AlTiS results with the gauging station. Our results show good correlation with those from AlTiS.

Table 3 summarizes $R^2$ and RMSE according to areas and sensors. Our automatic results give better $R^2$ and RMSE near Curuaí with Envisat sensor, whereas AlTiS results are better compared when using Saral data. Near Santos Dumont, AlTiS results are slightly better than automatic ones when using Envisat data. Finally, no automatic VS has been created over the river near Santos Dumont using Saral data, then comparisons with our method can't be possible but AlTiS and *in situ* method seems to be accurate enough.

## 5. Discussion

### *5.1. Identification of water regime along altimetry ground-tracks*

Through the use of k-means clustering and validation against reference land cover maps, we are able to attribute hydrological status

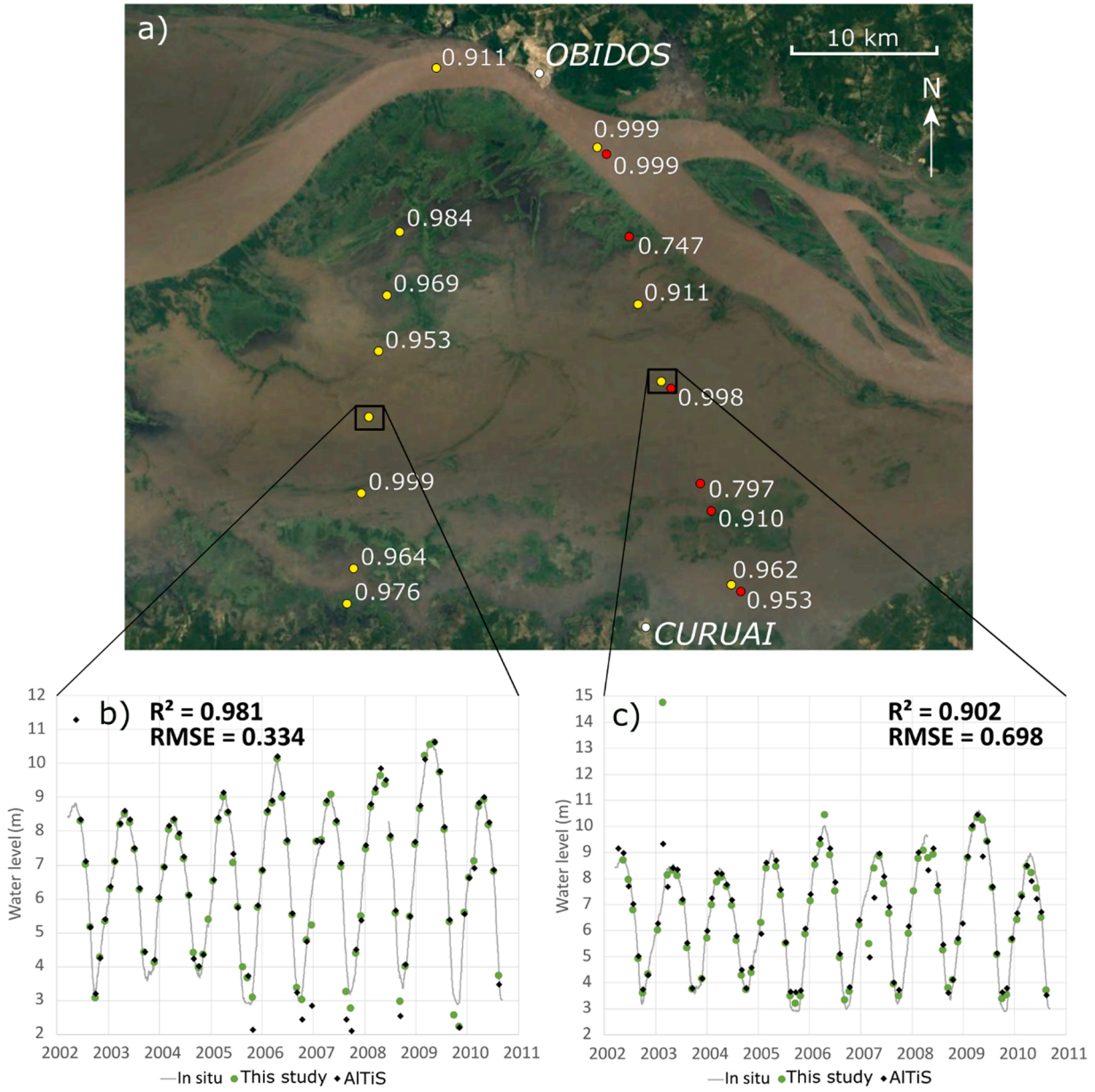


**Fig. 8.** – a) Location of automatically generated VS over Curuaí and $R^2$ associated (Yellow points = Envisat. Red points = Saral). b) and c) Examples of time series of WL from *in-situ* WL (grey line), automatically generated VS (green points), and manually generated (black lozenges). Biases with *in situ* gauges has been removed.

(open water, flooded and non-flooded areas) to each class. As in Frédéric Frappart et al. (2021c), our classifications and associated regimes coincide well with reference classes (Arantes et al., 2019; Hess et al., 2015). Class 0 is very often located on open water (lakes or rivers); on the contrary, class 3 is mainly located in non-flooded areas. Classes 1 and 2 correspond to intermediate hydrological environment such as permanently or seasonally flooded and seasonally or infrequently flooded, respectively. Nevertheless, reference land cover maps may be strongly methodology-dependant and thus may not be always accurate for our comparison. Indeed, the reference map over Curuaí from Arantes et al. (2019) has been obtained using Landsat (optical) images acquired between 2008 and 2009 and the one over Juruá river from Hess et al. (2015) has been obtained using SAR during the 1996 high water season (May to July), whereas Envisat and Saral respectively provide altimetry data over 2002–2010 and 2013–2016. This lack of time concordance may reduce accuracy classifications.

Best classifications are obtained with both B and B+NWL parameter, for both satellites but we focus on B+NWL results only to assess these new results. Envisat classifications are generally better than Saral's ones. Several reasons are likely to account for such lower accuracies of Saral results compared to Envisat's. The most obvious one is the drift of the Saral mission on its nominal orbit of

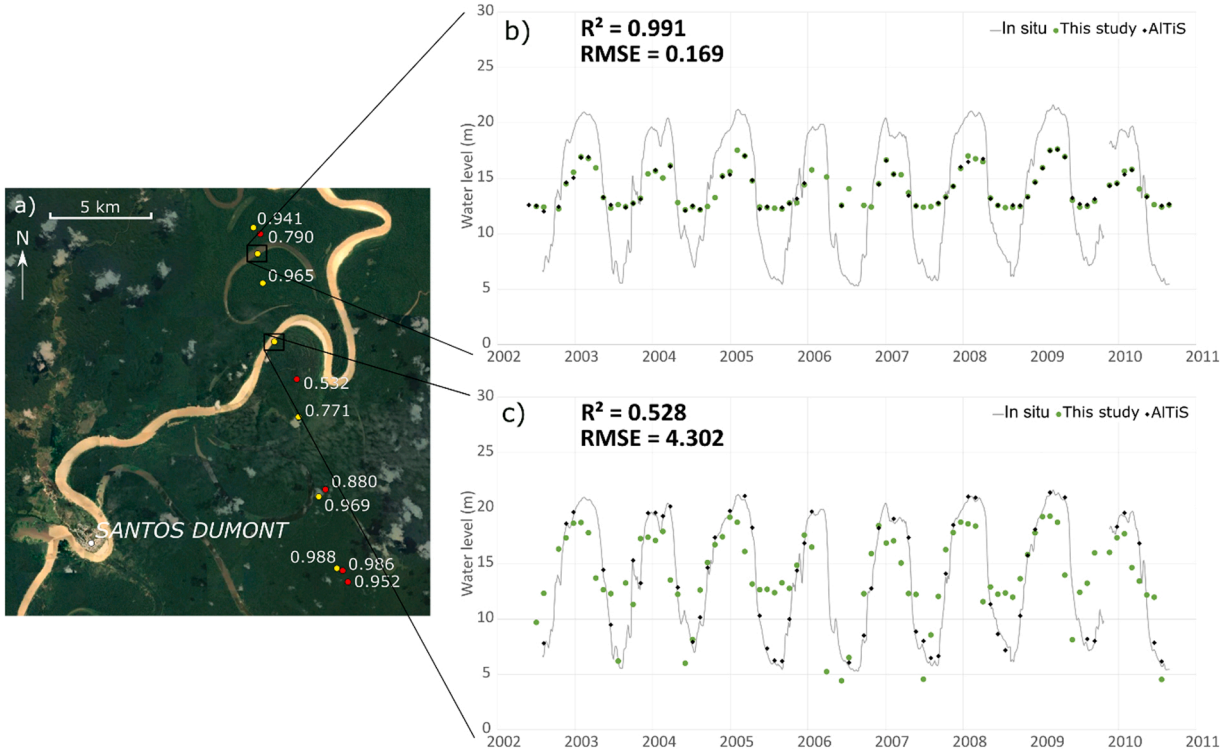


**Fig. 9.** – a) Location of automatically generated VS over the Juruá (Yellow points = Envisat. Red points = Saral). b) and c) Examples of time series of WL from *in-situ* WL (grey line), automatically generated VS (green points), and manually generated (black lozenges). Biases with *in situ* gauges has been removed.

**Table 3**
$R^2$ and RMSE results near to Curuaí and Santos Dumont gauge stations with Envisat and Saral sensors for WL time series comparisons.

| | | | $R^2$ | RMSE (m) |
|---|---|---|---|---|
| Envisat | Curuaí | Automatic/AlTiS | [0.90, 0.99] | [0.07, 0.70] |
| | | Automatic/*In situ* | 0.90 | 0.70 |
| | | AlTiS/*In situ* | 0.80 | 0.92 |
| | Juruá | Automatic/AlTiS | [0.52, 0.97] | [0.17, 4.30] |
| | | Automatic/*In Situ* | 0.75 | 2.89 |
| | | AlTiS/*In situ* | 0.83 | 2.49 |
| Saral | Curuaí | Automatic/AlTiS | [0.74, 0.99] | [0.06, 1.47] |
| | | Automatic/*In situ* | 0.69 | 1.94 |
| | | AlTiS/*In situ* | 0.79 | 1.07 |
| | Juruá | Automatic/AlTiS | [0.53, 0.98] | [0.36, 2.81] |
| | | Automatic/*In Situ* | X | X |
| | | AlTiS/*In situ* | 0.88 | 0.95 |

several kilometres. From one cycle to another, the land cover contained in the Saral footprint was different causing inaccuracies in the classification process. Another one is related to the great time-lag between reference maps period 1995–1996 Juruá and 2009–2010 for Curuaí . Finally, Saral is the first sensor to operate at Ka band. Larger scattering in the vegetation and more power backscattered at Ka band are measured by Saral than at Ku band, and then affect calculated accuracies.

### *5.2. VS creation and validation*

VS detection over Curuaí is effective. River width is up to 6 km and floodplain lakes are large enough to allow a good detection of open water in the radar footprint. However, the Juruá river is narrower, locally up to 400 m width downstream and up to 200 m width upstream, as well as abandoned meanders that are now lakes. Detection of water is therefore more difficult. Nevertheless, the virtual stations created are quite numerous, especially when using the B or B+NWL parameters. With this method, a significant densification of the virtual station network is therefore achieved. As a comparison, 6 VS from the Hydroweb database (http://hydroweb.theialand.fr/) are available over the Amazon in Curuaí region, while about 100 VS have been created over the river and floodplains with our

method. For the Juruá, more than 100 VS from the Hydroweb database are available over the river, while about 1500 VS have been created over the river and floodplains. The backscatter coefficient parameter combined with the raw water levels (B+RWL) did not give satisfying results either for classification accuracies or for number of VS created. This may be due to the extreme changes between water levels over the different surface types.

A bias of almost 2 m can be observed for Envisat data and 1.5 m for Saral data over Curuaí and has been respectively removed. Previous studies showed that Envisat has a + 1 m bias compared to *in situ* gauges (Calmant et al., 2013; Santos da Silva et al., 2010). Still, part of the bias could be due to the distance between automatic VS and *in situ* gauges. Nevertheless, $R^2$ and RMSE are estimated and show good agreement between the automatic time series and AlTiS ones.

As over the Congo river (Frappart et al., 2021c), the automatic method over Amazon's forest is more efficient than the manual AlTiS software. Indeed, automatic method is faster than AlTiS computation and allow monitoring floodplains areas. Moreover, removing outliers from AlTiS software induce fewer elements in time series. Despite the slightly worse $R^2$ and RMSE results than for Curuaí , the method is rather effective in Santos Dumont. However, as it can be seen in Fig. 9.c), Juruá river automatic results should be considered with caution. Juruá river and ancient meanders are well detected using Envisat data. But, during low water period, some anomalous water levels can be retrieved most probably due to the narrowness of the river.

### 5.3. River-floodplain connectivity

Using the automatically generated WL series, it is possible to carry out a connectivity analysis between floodplain lakes and rivers by examining the duration of the connection between the mainstream and the lakes (or between lakes) during floods and recessions, detecting different filling/emptying dynamics between lakes. The methodology that leads to an important densification of the number of water level measurement points in rivers and floodplains is an important contribution for the scientific community to better understand the dynamics of river-floodplain exchanges and their evolution over time.

With this method, the new densified VS network permits to obtain information on water bodies WL along the river and along river cross-sections, enabling to analyse hydrologic connectivity between river and lakes and lakes with each other and determine flood duration and rising/draining velocities at each VS. As an example, VS time series in the river and the Curuaí floodplain, created using Envisat data (B+NWL parameter), are shown in Fig. 10a. Most of the time, the river is flooded before the floodplain, except for some years during which the flood is beginning earlier (*e.g.* 2006, 2007) and can last from 6 to 8 months depending on the year, generally from November/December to May/June. Mean rising velocity is about 0.8 m/month in the river and in the floodplain, except in the Lago Grande do Curuaí where the flood is slower (0.7 m/month). Then, falling phase is beginning and can last from 4.5 to 7 months depending on the year, generally until November/December. Draining velocities are about 1 m/month in the river and in the floodplain, except in the Lago Grande do Curuaí where the flood is slower (0.9 m/month). Indeed, west of the floodplain is flooded by the upstream river and small channels before the east which is flooded both by the west floodplain and by channels connected to the downstream river (Bonnet et al., 2008; Park and Latrubesse, 2017). The double input of east floodplain by the channels/river is easily seen for some years with the double peaks in the time series (*e.g.* 2003, 2004, 2008, 2009). VS time series in the Juruá river and the floodplain near Santos Dumont, created from Envisat (B+NWL parameter), are shown in Fig. 10b. Rising can last from 5 to 8 months depending on the year, generally from ~September to March/April. Rising velocity is about 1.2 m/month in the river, whereas they are slower (0.4–0.7 m/month) in the floodplain. Then, falling phase is beginning and can last from 4.5 to 8 months depending on the year, generally until ~September. Draining velocity is about 1.4 m/month in the river, whereas they are slower (0.5–0.7 m/month) in the floodplain. In this case, river is always flooded first and propagation of rising water in the floodplains is well seen after the flood begun several months ago. Times of connection can be easily recognised when the river is low. From the moment when flood begin until the floodplains is rising, four months has past (*e.g.* 2003, 2004, 2006, 2007). Times of disconnection between the river and the floodplains are lasting about 6 months in this Juruá portion.

This kind of information, coupled with bathymetry, can possibly permit to better interpret fish population dynamics (Hurd et al., 2016; Park and Latrubesse, 2017). Even if Envisat and Saral allow to analyse surface water connectivity at monthly time-scale, the opportunity of the new Ka-band wide-swath radar altimeter of the Surface Water and Ocean Topography (SWOT) mission will be unique (Biancamaria et al., 2016). Owing to its capability to map water levels at 100 m of spatial resolution several times during its 21-day repeat period, this new dataset will allow a finer monitoring of the surface water connectivity between river and floodplains.

## 6. Conclusion

In this study, we confirm the strong potential of radar altimetry backscattering coefficient to identify land water surfaces along the tracks. Compared to a previous study, we showed that the discrimination between land and water is enhanced when taking into consideration in the classification process the normalized water level in areas with a complex hydrodynamics such as the Curuaí várzea and the Juruá watershed, in Amazon. Results show good replicability and efficiency over a densely vegetated equatorial area. Indeed, classification accuracies of 0.74 (0.53) and 0.69 (0.59) were obtained for Envisat (Saral) when comparing with reference land cover maps in the Curuaí várzea and the Juruá watershed, respectively, using a k-means clustering approach. Based on these results, WL time series were automatically generated along the tracks over the classes associated to open water and inundation. Their creation permitted to strongly densify VS network in the river and the floodplains: 4650 VS were created in both areas. Comparisons show an accuracy ranging from 0.52 (0.53) to 0.97 (0.98) when comparing the time series of WL automatically generated with Envisat (Saral) with ones from the *in situ* station or the ones manually created in the Curuaí várzea.

On the one hand, this method offers possibility to include floodplain water level in current database and allow better surface water

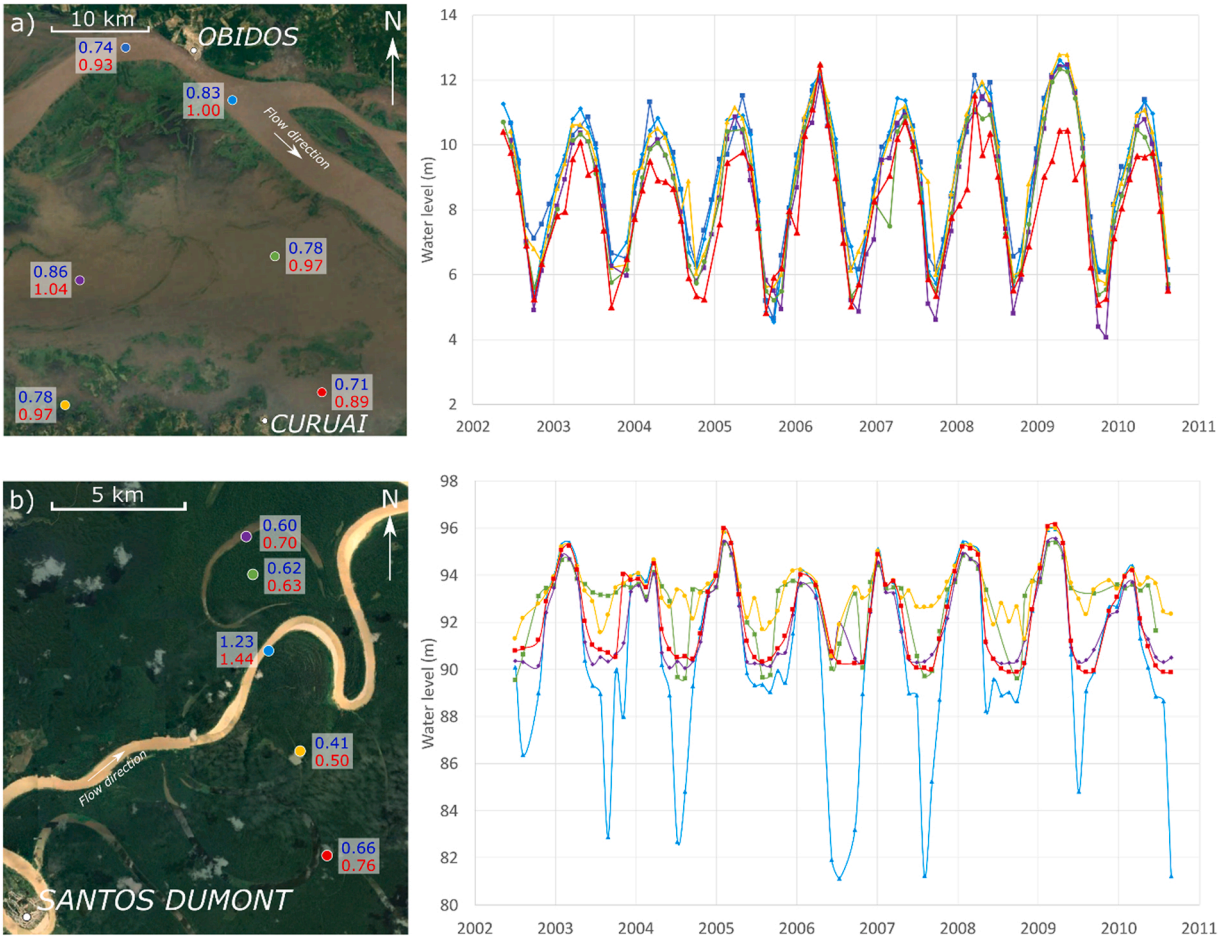


**Fig. 10.** – B+NWL parameter time series evolution from Envisat data in a) the Curuaí floodplain and in b) the flooded forest near to Santos Dumont along the Juruá. Blue and red strings are mean flood and mean drainage velocities in meter per month, respectively. Time series colours are map linked.

stock estimations to monitor areas where *in situ* data does not exist. On the other hand, the created WLs allow a better connectivity analysis between the river, the lakes and the floodplains. The wetlands' filling dynamic is better understood. Especially in Curuaí , where the varzea is filled to the west first *via* the upstream river, and then to the east *via* channels connected to the western floodplain and the downstream river. This information, coupled with bathymetry, would allow to better understand fish population dynamics and floodplain biogeochemical functioning. The recent launch of the SWOT mission offers new opportunities for better monitoring the channel-floodplains connectivity as this new mission will provide water level maps at 100 m of spatial resolution 2 or 3 times every 21 days in equatorial areas.

## CRediT authorship contribution statement

**Pauline Enguehard:** Conceptualization, Software, Validation, Investigation, Writing – original draft, Writing – review & editing, Visualization. **Frédéric Frappart:** Conceptualization, Software, Validation, Writing – original draft, Writing – review & editing, Supervision, Funding acquisition. **Pierre Zeiger:** Methodology, Software. **Fabien Blarel**: Methodology, Resources. **Frédéric Satgé:** Conceptualization, Funding acquisition. **Marie-Paule Bonnet:** Conceptualization, Writing – original draft, Supervision, Funding acquisition.

## Declaration of Competing Interest

The authors declare that they have no known competing financial interests or personal relationships that could have appeared to influence the work reported in this paper.

## Data Availability

The data and related documentations that support the findings of this study are openly available in DataSuds repository (IRD, France) at https://doi.org/10.23708/HOZKPW . Data reuse is granted under CC-BY license.

## Acknowledgments

The first author is grateful to the Occitanie region, SABERES project (BNP Paribas foundation 2020–2025) and WASACA (Agropolis foundation) fundings. This research is funded in the framework of the BONDS (Balancing biOdiversity coNservation and Development in Amazon wetlandS) project funded through the 2017–2018 Belmont Forum and BiodivERsA joint call for research proposals, under the BiodivScen ERA-Net COFUND programme, and with the funding organisations French National Research Agency (ANR), São Paulo Research Foundation (FAPESP), National Science Foundation (NSF), the Research Council of Norway and the German Federal Ministry of Education and Research (BMBF). This research is also a contribution the CNES's TOSCA SWOT SWHYM project.

## Appendix A. Supporting information

Supplementary data associated with this article can be found in the online version at doi:10.1016/j.ejrh.2023.101397.

## References

Abdalla, S., Abdeh Kolahchi, A., Ablain, M., Adusumilli, S., Aich Bhowmick, S., Alou-Font, E., Amarouche, L., Andersen, O.B., Antich, H., Aouf, L., Arbic, B., Armitage, T., Arnault, S., Artana, C., Aulicino, G., Ayoub, N., Badulin, S., Baker, S., Banks, C., Bao, L., Barbetta, S., Barceló-Llull, B., Barlier, F., Basu, S., Bauer-Gottwein, P., Becker, M., Beckley, B., Bellefond, N., Belonenko, T., Benkiran, M., Benkouider, T., Bennartz, R., Benveniste, J., Bercher, N., Berge-Nguyen, M., Bettencourt, J., Blarel, F., Blazquez, A., Blumstein, D., Bonnefond, P., Borde, F., Bouffard, J., Boy, F., Boy, J.-P., Brachet, C., Brasseur, P., Braun, A., Brocca, L., Brockley, D., Brodeau, L., Brown, S., Bruinsma, S., Bulczak, A., Buzzard, S., Cahill, M., Calmant, S., Calzas, M., Camici, S., Cancet, M., Capdeville, H., Carabajal, C. C., Carrere, L., Cazenave, A., Chassignet, E.P., Chauhan, P., Cherchali, S., Chereskin, T., Cheymol, C., Ciani, D., Cipollini, P., Cirillo, F., Cosme, E., Coss, S., Cotroneo, Y., Cotton, D., Couhert, A., Coutin-Faye, S., Crétaux, J.-F., Cyr, F., d'Ovidio, F., Darrozes, J., David, C., Dayoub, N., De Staerke, D., Deng, X., Desai, S., Desjonqueres, J.-D., Dettmering, D., Di Bella, A., Díaz-Barroso, L., Dibarboure, G., Dieng, H.B., Dinardo, S., Dobslaw, H., Dodet, G., Doglioli, A., Domeneghetti, A., Donahue, D., Dong, S., Donlon, C., Dorandeu, J., Drezen, C., Drinkwater, M., Du Penhoat, Y., Dushaw, B., Egido, A., Erofeeva, S., Escudier, P., Esselborn, S., Exertier, P., Fablet, R., Falco, C., Farrell, S.L., Faugere, Y., Femenias, P., Fenoglio, L., Fernandes, J., Fernández, J.G., Ferrage, P., Ferrari, R., Fichen, L., Filippucci, P., Flampouris, S., Fleury, S., Fornari, M., Forsberg, R., Frappart, F., Frery, M., Garcia, P., Garcia-Mondejar, A., Gaudelli, J., Gaultier, L., Getirana, A., Gibert, F., Gil, A., Gilbert, L., Gille, S., Giulicchi, L., Gómez-Enri, J., Gómez-Navarro, L., Gommenginger, C., Gourdeau, L., Griffin, D., Groh, A., Guerin, A., Guerrero, R., Guinle, T., Gupta, P., Gutknecht, B.D., Hamon, M., Han, G., Hauser, D., Helm, V., Hendricks, S., Hernandez, F., Hogg, A., Horwath, M., Idžanović, M., Janssen, P., Jeansou, E., Yongjun, Jia, Yuanyuan, Jia, Jiang, L., Johannessen, J.A., Kamachi, M., Karimova, S., Kelly, K., Kim, S.Y., King, R., Kittel, C.M.M., Klein, P., Klos, A., Knudsen, P., Koenig, R., Kostianoy, A., Kouraev, A., Kumar, R., Labroue, S., Lago, L.S., Lambin, J., Lasson, L., Laurain, O., Laxenaire, R., Lázaro, C., Le Gac, S., Le Sommer, J., Le Traon, P.-Y., Lebedev, S., Léger, F., Legresy, B., Lemoine, F., Lenain, L., Leuliette, E., Levy, M., Lillibridge, J., Liu, J., Llovel, W., Lyard, F., Macintosh, C., Makhoul Varona, E., Manfredi, C., Marin, F., Mason, E., Massari, C., Mavrocordatos, C., Maximenko, N., McMillan, M., Medina, T., Melet, A., Meloni, M., Mertikas, S., Metref, S., Meyssignac, B., Minster, J.-F., Moreau, T., Moreira, D., Morel, Y., Morrow, R., Moyard, J., Mulet, S., Naeije, M., Nerem, R.S., Ngodock, H., Nielsen, K., Nilsen, J.E.Ø., Niño, F., Nogueira Loddo, C., Noûs, C., Obligis, E., Otosaka, I., Otten, M., Oztunali Ozbahceci, B., Raj, P., Paiva, R., Paniagua, R., Paolo, G., Paris, F., Pascual, A., Passaro, A., Paul, M., Pavelsky, S., Pearson, T., Penduff, C., Peng, T., Perosanz, F., Picot, F., Piras, N., Poggiali, F., Poirier, V., Ponce de León, É., Prants, S., Prigent, S., Provost, C., Pujol, C., Qiu, M.-I., Quilfen, B., Rami, Y., Raney, A., Raynal, R.K., Remy, M., Rémy, E., Restano, F., Richardson, M., Richardson, A., Ricker, D., Ricko, R., Rinne, M., Rose, E., Rosmorduc, S.K., Rudenko, V., Ruiz, S., Ryan, S., Salaün, B.J., Sanchez-Roman, C., Sandberg Sørensen, A., Sandwell, L., Saraceno, D., Scagliola, M., Schaeffer, M., Scharffenberg, P., Scharroo, M.G., Schiller, R., Schneider, A., Schwatke, R., Scozzari, C., Ser-giacomi, A., Seyler, E., Shah, F., Sharma, R., Shaw, R., Shepherd, A., Shriver, A., Shum, J., Simons, C.K., Simonsen, W., Slater, S.B., Smith, T., Soares, W., Sokolovskiy, S., Soudarin, M., Spatar, L., Speich, C., Srinivasan, S., Srokosz, M., Stanev, M., Staneva, E., Steunou, J., Stroeve, N., Su, J., Sulistioadi, B., Swain, Y.B., Sylvestre-baron, D., Taburet, A., Tailleux, N., Takayama, R., Tapley, K., Tarpanelli, B., Tavernier, A., Testut, G., Thakur, L., Thibaut, P.K., Thompson, P., Tintoré, L., Tison, J., Tourain, C., Tournadre, C., Townsend, J., Tran, B., Trilles, N., Tsamados, S., Tseng, M., Ubelmann, K.-H., Uebbing, C., Vergara, B., Verron, O., Vieira, J., Vignudelli, T., Vinogradova Shiffer, S., Visser, N., Vivier, P., Volkov, F., von Schuckmann, D., Vuglinskii, K., Vuilleumier, V., Walter, P., Wang, B., Wang, J., Watson, C., Wilkin, C., Willis, J., Wilson, J., Woodworth, H., Yang, P., Yao, K., Zaharia, F., Zakharova, R., Zaron, E., Zhang, E.D., Zhao, Y., Zinchenko, Z., V., Zlotnicki, V, 2021. Altimetry for the future: building on 25 years of progress. Advances in Space Research. https://doi.org/10.1016/j.asr.2021.01.022.

Alsdorf, D., Birkett, C., Dunne, T., Melack, J., Hess, L., 2001. Water level changes in a large Amazon lake measured with spaceborne radar interferometry and altimetry. Geophys. Res. Lett. 28, 2671–2674. https://doi.org/10.1029/2001GL012962.

Alsdorf, D.E., Melack, J.M., Dunne, T., Mertes, L.A.K., Hess, L.L., Smith, L.C., 2000. Interferometric radar measurements of water level changes on the Amazon flood plain. Nature 404, 174–177. https://doi.org/10.1038/35004560.

Alsdorf, D.E., Rodríguez, E., Lettenmaier, D.P., 2007. Measuring surface water from space. Rev. Geophys. 45, RG2002. https://doi.org/10.1029/2006RG000197.

AlTiS data request — CTOH [WWW Document], n.d. URL http://ctoh.legos.obs-mip.fr/applications/land_surfaces/altimetric_data/altis (accessed 1.9.23).

Arantes, C.C., Winemiller, K.O., Asher, A., Castello, L., Hess, L.L., Petrere, M., Freitas, C.E.C., 2019. Floodplain land cover affects biomass distribution of fish functional diversity in the Amazon River. Sci. Rep. 9, 16684. https://doi.org/10.1038/s41598-019-52243-0.

Arnesen, A.S., Silva, T.S.F., Hess, L.L., Novo, E.M.L.M., Rudorff, C.M., Chapman, B.D., McDonald, K.C., 2013. Monitoring flood extent in the lower Amazon River floodplain using ALOS/PALSAR ScanSAR images. Remote Sens. Environ. 130, 51–61. https://doi.org/10.1016/j.rse.2012.10.035.

Benveniste, J., Milagro-Perez, M.P., Roca, M., Levrini, G., 2003. The ENVISAT Radar Altimeter System. In: Hwang, C., Shum, C.K., Li, J. (Eds.), Satellite Altimetry for Geodesy, Geophysics and Oceanography, International Association of Geodesy Symposia. Springer Berlin Heidelberg, Berlin, Heidelberg, pp. 251–259. https://doi.org/10.1007/978-3-642-18861-9_31.

Biancamaria, S., Lettenmaier, D.P., Pavelsky, T.M., 2016. The SWOT mission and its capabilities for land hydrology. Surv. Geophys 37, 307–337. https://doi.org/10.1007/s10712-015-9346-y.

Bonnefond, P., Verron, J., Aublanc, J., Babu, K., Bergé-Nguyen, M., Cancet, M., Chaudhary, A., Crétaux, J.-F., Frappart, F., Haines, B., Laurain, O., Ollivier, A., Poisson, J.-C., Prandi, P., Sharma, R., Thibaut, P., Watson, C., 2018. The benefits of the Ka-band as evidenced from the SARAL/AltiKa altimetric mission: quality assessment and unique characteristics of AltiKa Data. Remote Sens. 10, 83. https://doi.org/10.3390/rs10010083.

Bonnet, M.P., Barroux, G., Martinez, J.M., Seyler, F., Moreira-Turcq, P., Cochonneau, G., Melack, J.M., Boaventura, G., Maurice-Bourgoin, L., León, J.G., Roux, E., Calmant, S., Kosuth, P., Guyot, J.L., Seyler, P., 2008. Floodplain hydrology in an Amazon floodplain lake (Lago Grande de Curuaí). J. Hydrol. 349, 18–30. https://doi.org/10.1016/j.jhydrol.2007.10.055.

Callede, J., Guyot, J.L., Ronchail, J., Molinier, M., De Oliveira, E., 2002. L'Amazone à Óbidos (Brésil): étude statistique des débits et bilan hydrologique. Hydrol. Sci. J. 47, 321–333. https://doi.org/10.1080/02626660209492933.

Calmant, S., da Silva, J.S., Moreira, D.M., Seyler, F., Shum, C.K., Crétaux, J.F., Gabalda, G., 2013. Detection of Envisat RA2/ICE-1 retracked radar altimetry bias over the Amazon basin rivers using GPS. Adv. Space Res. 51, 1551–1564. https://doi.org/10.1016/j.asr.2012.07.033.

Costanza, R., d'Arge, R., de Groot, R., Farber, S., Grasso, M., Hannon, B., Limburg, K., Naeem, S., O'Neill, R.V., Paruelo, J., Raskin, R.G., Sutton, P., van den Belt, M., 1997. The value of the world's ecosystem services and natural capital. Nature 387, 253–260. https://doi.org/10.1038/387253a0.

Cretaux, J.-F., Nielsen, K., Frappart, F., Papa, F., Calmant, S., Benveniste, J., 2017. Hydrological Applications of Satellite AltimetryRivers, Lakes, Man-Made Reservoirs, Inundated Areas, in: Stammer, D., Cazenave, A. (Eds.), Satellite Altimetry over Oceans and Land Surfaces. CRC Press, Boca Raton, FL: Taylor & Francis, 2017., pp. 459–504. https://doi.org/10.1201/9781315151779–14.

Davidson, N.C., Fluet-Chouinard, E., Finlayson, C.M., 2018. Global extent and distribution of wetlands: trends and issues. Mar. Freshw. Res. 69, 620. https://doi.org/10.1071/MF17019.

Denny, P., 1994. Biodiversity and wetlands. Wetl. Ecol. Manag. 3. https://doi.org/10.1007/BF00177296.

Dubos, N., Lenormand, M., Castello, L., Oberdorff, T., Guisan, A., Luque, S., 2022. Protection gaps in Amazon floodplains will increase with climate change: Insight from the world's largest scaled freshwater fish. Aquat. Conserv. aqc 3877. https://doi.org/10.1002/aqc.3877.

Dudgeon, D., Arthington, A.H., Gessner, M.O., Kawabata, Z.-I., Knowler, D.J., Lévêque, C., Naiman, R.J., Prieur-Richard, A.-H., Soto, D., Stiassny, M.L.J., Sullivan, C. A., 2006. Freshwater biodiversity: importance, threats, status and conservation challenges. Biol. Rev. 81, 163. https://doi.org/10.1017/S1464793105006950.

Enguehard, P., Frappart, F., Zeiger, P., Blarel, F., Satge, F., Bonnet, M.-P., 2023. Water Lev. Stations Amaz. floodplains Radar echoes Classif. https://doi.org/10.23708/HOZKPW.

Fassoni-Andrade, A.C., Paiva, R.C.D., de, Rudorff, C., de, M., Barbosa, C.C.F., Novo, E.M.L., de, M., 2020. High-resolution mapping of floodplain topography from space: a case study in the Amazon. Remote Sens. Environ. 251, 112065 https://doi.org/10.1016/j.rse.2020.112065.

Foley, J.A., Asner, G.P., Costa, M.H., Coe, M.T., DeFries, R., Gibbs, H.K., Howard, E.A., Olson, S., Patz, J., Ramankutty, N., Snyder, P., 2007. Amazonia revealed: forest degradation and loss of ecosystem goods and services in the Amazon Basin. Front. Ecol. Environ. 5, 25–32. https://doi.org/10.1890/1540-9295(2007)5[25:ARFDAL]2.0.CO;2.

Frappart, F., Calmant, S., Cauhope, M., Seyler, F., Cazenave, A., 2006. Preliminary results of ENVISAT RA-2-derived water levels validation over the Amazon basin. Remote Sens. Environ. 100, 252–264. https://doi.org/10.1016/j.rse.2005.10.027.

Frappart, F., Fatras, C., Mougin, E., Marieu, V., Diepkilé, A.T., Blarel, F., Borderies, P., 2015a. Radar altimetry backscattering signatures at Ka, Ku, C, and S bands over West Africa. Phys. Chem. Earth, Parts A/B/C. 83–84, 96–110. https://doi.org/10.1016/j.pce.2015.05.001.

Frappart, F., Papa, F., Marieu, V., Malbeteau, Y., Jordy, F., Calmant, S., Durand, F., Bala, S., 2015b. Preliminary assessment of SARAL/AltiKa observations over the Ganges-Brahmaputra and Irrawaddy Rivers. Mar. Geod. 38, 568–580. https://doi.org/10.1080/01490419.2014.990591.

Frappart, Frédéric, Blarel, F., Fayad, I., Bergé-Nguyen, M., Crétaux, J.-F., Shu, S., Schregenberger, J., Baghdadi, N., 2021a. Evaluation of the performances of radar and lidar altimetry missions for water level retrievals in mountainous environment: the case of the Swiss Lakes. Remote Sens. 13, 2196. https://doi.org/10.3390/rs13112196.

Frappart, Frédéric, Blarel, F., Papa, F., Prigent, C., Mougin, E., Paillou, P., Baup, F., Zeiger, P., Salameh, E., Darrozes, J., Bourrel, L., Rémy, F., 2021b. Backscattering signatures at Ka, Ku, C and S bands from low resolution radar altimetry over land. Adv. Space Res. 68, 989–1012. https://doi.org/10.1016/j.asr.2020.06.043.

Frappart, Frédéric, Zeiger, P., Betbeder, J., Gond, V., Bellot, R., Baghdadi, N., Blarel, F., Darrozes, J., Bourrel, L., Seyler, F., 2021c. Automatic detection of inland water bodies along altimetry tracks for estimating surface water storage variations in the Congo Basin. Remote Sens. 13, 3804. https://doi.org/10.3390/rs13193804.

Hess, L., 2003. Dual-season mapping of wetland inundation and vegetation for the central Amazon basin. Remote Sens. Environ. 87, 404–428. https://doi.org/10.1016/j.rse.2003.04.001.

Hess, L.L., Melack, J.M., Affonso, A.G., Barbosa, C., Gastil-Buhl, M., Novo, E.M.L.M., 2015. Wetlands of the lowland Amazon basin: extent, vegetative cover, and dual-season inundated area as mapped with JERS-1 synthetic aperture radar. Wetlands 35, 745–756. https://doi.org/10.1007/s13157-015-0666-y.

Hidro-Telemetria / Mapa [WWW Document], n.d. URL https://www.snirh.gov.br/hidrotelemetria/Mapa.aspx (accessed 1.9.23).

Hurd, L.E., Sousa, R.G.C., Siqueira-Souza, F.K., Cooper, G.J., Kahn, J.R., Freitas, C.E.C., 2016. Amazon floodplain fish communities: habitat connectivity and conservation in a rapidly deteriorating environment. Biol. Conserv. 195, 118–127. https://doi.org/10.1016/j.biocon.2016.01.005.

Hydroweb [WWW Document], n.d. URL https://hydroweb.theia-land.fr/ (Accessed 1 September 23).

Jain, A.K., Dubes, R.C., 1988. Algorithms for Clustering Data. ed. Prentice-Hall, Inc.

Janse, J.H., van Dam, A.A., Hes, E.M.A., de Klein, J.J.M., Finlayson, C.M., Janssen, A.B.G., van Wijk, D., Mooij, W.M., Verhoeven, J.T.A., 2019. Towards a global model for wetlands ecosystem services. Curr. Opin. Environ. Sustain. 36, 11–19. https://doi.org/10.1016/j.cosust.2018.09.002.

Jézéquel, C., Tedesco, P.A., Darwall, W., Dias, M.S., Frederico, R.G., Hidalgo, M., Hugueny, B., Maldonado-Ocampo, J., Martens, K., Ortega, H., Torrente-Vilara, G., Zuanon, J., Oberdorff, T., 2020. Freshwater fish diversity hotspots for conservation priorities in the Amazon Basin. Conserv. Biol. 34, 956–965. https://doi.org/10.1111/cobi.13466.

Jisha, K.C., Puthur, J.T., 2021. Ecological importance of wetland systems, in: Wetlands Conservation.

Jung, H.C., Hamski, J., Durand, M., Alsdorf, D., Hossain, F., Lee, H., Hossain, A.K.M.A., Hasan, K., Khan, A.S., Hoque, A.K.M.Z., 2010. Characterization of complex fluvial systems using remote sensing of spatial and temporal water level variations in the Amazon, Congo, and Brahmaputra Rivers. Earth Surf. Process. Landf. 35, 294–304. https://doi.org/10.1002/esp.1914.

Junk, W.J., Bayley, P.B., Sparks, R.E., 1989. The flood pulse concept in river-floodplain systems. Fish. Aquat. Sci. 106, 110–127.

Junk, W.J., Piedade, M.T.F., Lourival, R., Wittmann, F., Kandus, P., Lacerda, L.D., Bozelli, R.L., Esteves, F.A., Nunes da Cunha, C., Maltchik, L., Schöngart, J., Schaeffer-Novelli, Y., Agostinho, A.A., 2014. Brazilian wetlands: their definition, delineation, and classification for research, sustainable management, and protection: BRAZILIAN WETLANDS. Aquatic Conserv: Mar. Freshw. Ecosyst. 24, 5–22. https://doi.org/10.1002/aqc.2386.

Kodinariya, T.M., Makwana, P.R., 2013. Review on determining number of cluster in K-means clustering. Int. J. 1, 90–95.

Latrubesse, E.M., Arima, E.Y., Dunne, T., Park, E., Baker, V.R., d'Horta, F.M., Wight, C., Wittmann, F., Zuanon, J., Baker, P.A., Ribas, C.C., Norgaard, R.B., Filizola, N., Ansar, A., Flyvbjerg, B., Stevaux, J.C., 2017. Damming the rivers of the Amazon basin. Nature 546, 363–369. https://doi.org/10.1038/nature22333.

Likas, A., Vlassis, N., Verbeek, J, J., 2003. The global k-means clustering algorithm. Pattern Recognit. 36, 451–461. https://doi.org/10.1016/S0031-3203(02)00060-2.

Marengo, J.A., Espinoza, J.C., 2016. Extreme seasonal droughts and floods in Amazonia: causes, trends and impacts: EXTREMES IN AMAZONIA. Int. J. Clim. 36, 1033–1050. https://doi.org/10.1002/joc.4420.

Melack, J.M., Hess, L.L., 2010. Remote sensing of the distribution and extent of wetlands in the Amazon basin. In: Junk, W.J., Piedade, M.T.F., Wittmann, F., Schöngart, J., Parolin, P. (Eds.), Amazonian Floodplain Forests. Springer, Netherlands, Dordrecht, pp. 43–59. https://doi.org/10.1007/978-90-481-8725-6_3.

Melack, J.M., Kasper, D., Amaral, J.H.F., Barbosa, P.M., Forsberg, B.R., 2021. Limnological perspectives on conservation of floodplain lakes in the Amazon basin. Aquat. Conserv. 31, 1041–1055. https://doi.org/10.1002/aqc.3556.

Moomaw, W.R., Chmura, G.L., Davies, G.T., Finlayson, C.M., Middleton, B.A., Natali, S.M., Perry, J.E., Roulet, N., Sutton-Grier, A.E., 2018. Wetlands In a changing climate: science, policy and management. Wetlands 38, 183–205. https://doi.org/10.1007/s13157-018-1023-8.

Mota Da Silva, P.J., 2020. Channel pattern and flow rate analyses of the Juruá River. Northwest Bras. Rev. De. Geol. 33, 103–110.

Normandin, C., Frappart, F., Diepkilé, A.T., Marieu, V., Mougin, E., Blarel, F., Lubac, B., Braquet, N., Ba, A., 2018. Evolution of the performances of radar altimetry missions from ERS-2 to sentinel-3A over the Inner Niger Delta. Remote Sens. 10, 833. https://doi.org/10.3390/rs10060833.

ORNL DAAC for Biogeochemical Dynamics [WWW Document], n.d. URL https://daac.ornl.gov/ (accessed 1.9.23).

Papa, F., Frappart, F., 2021. Surface water storage in rivers and wetlands derived from satellite observations: a review of current advances and future opportunities for hydrological sciences. Remote Sens. 13, 4162. https://doi.org/10.3390/rs13204162.

Park, E., 2020. Characterizing channel-floodplain connectivity using satellite altimetry: mechanism, hydrogeomorphic control, and sediment budget. Remote Sens. Environ. 243, 111783 https://doi.org/10.1016/j.rse.2020.111783.

Park, E., Latrubesse, E.M., 2017. The hydro-geomorphologic complexity of the lower Amazon River floodplain and hydrological connectivity assessed by remote sensing and field control. Remote Sens. Environ. 198, 321–332. https://doi.org/10.1016/j.rse.2017.06.021.

Pavlis, N.K., Holmes, S.A., Kenyon, S.C., Factor, J.K., 2012. The development and evaluation of the earth gravitational model 2008 (EGM2008): THE EGM2008 earth gravitational modeL, 117, n/a-n/a J. Geophys. Res. https://doi.org/10.1029/2011JB008916.

Rast, M., Johannessen, J., Mauser, W., 2014. Review of understanding of earth's hydrological cycle: observations, theory and modelling. Surv. Geophys 35, 491–513. https://doi.org/10.1007/s10712-014-9279-x.

Santos da Silva, J., Calmant, S., Seyler, F., Rotunno Filho, O.C., Cochonneau, G., Mansur, W.J., 2010. Water levels in the Amazon basin derived from the ERS 2 and ENVISAT radar altimetry missions. Remote Sens. Environ. 114, 2160–2181. https://doi.org/10.1016/j.rse.2010.04.020.

Shu, S., Liu, H., Beck, R.A., Frappart, F., Korhonen, J., Lan, M., Xu, M., Yang, B., Huang, Y., 2021. Evaluation of historic and operational satellite radar altimetry missions for constructing consistent long-term lake water level records. Hydrol. Earth Syst. Sci. 25, 1643–1670. https://doi.org/10.5194/hess-25-1643-2021.

da Silva, M.T., Pereira, J., de, O., Vieira, L.J.S., Petry, A.C., 2013. Hydrological seasonality of the river affecting fish community structure of oxbow lakes: a limnological approach on the Amapá Lake, southwestern Amazon. Limnologica 43, 79–90. https://doi.org/10.1016/j.limno.2012.05.002.

da Silva Abel, E.L., Delgado, R.C., Vilanova, R.S., Teodoro, P.E., da Silva Junior, C.A., Abreu, M.C., Silva, G.F.C., 2021. Environmental dynamics of the Juruá watershed in the Amazon. Environ. Dev. Sustain 23, 6769–6785. https://doi.org/10.1007/s10668-020-00890-z.

Sousa, M.M., Oliveira, W., 2016. Identificação de feições anômalas dos sistemas de drenagem na região do Alto Juruá – AC/AM, utilizando dados de sensoriamento remoto. Rev. Bras. De. Geogr. Física 9, 1254–1267.

Satellite altimetry over oceans and land surfaces. In: Stammer, D., Cazenave, A. (Eds.), 2017. Earth observation of global changes. CRC Press, Taylor & Francis Group, Boca Raton London New York.

Trigg, M.A., Bates, P.D., Wilson, M.D., Schumann, G., Baugh, C., 2012. Floodplain channel morphology and networks of the middle Amazon River. Water Resour. Res. 48, 2012WR011888. https://doi.org/10.1029/2012WR011888.

Verron, J., Sengenes, P., Lambin, J., Noubel, J., Steunou, N., Guillot, A., Picot, N., Coutin-Faye, S., Sharma, R., Gairola, R.M., Murthy, D.V.A.R., Richman, J.G., Griffin, D., Pascual, A., Rémy, F., Gupta, P.K., 2015. The SARAL/AltiKa altimetry satellite mission. Mar. Geod. 38, 2–21. https://doi.org/10.1080/01490419.2014.1000471.

Verron, J., Bonnefond, P., Andersen, O., Ardhuin, F., Bergé-Nguyen, M., Bhowmick, S., Blumstein, D., Boy, F., Brodeau, L., Crétaux, J.-F., Dabat, M.L., Dibarboure, G., Fleury, S., Garnier, F., Gourdeau, L., Marks, K., Queruel, N., Sandwell, D., Smith, W.H.F., Zaron, E.D., 2021. The SARAL/AltiKa mission: A step forward to the future of altimetry. Adv. Space Res. 68, 808–828. https://doi.org/10.1016/j.asr.2020.01.030.

Vorosmarty, C., Askew, A., Grabs, W., Barry, R.G., Birkett, C., Doll, P., Goodison, B., Hall, A., Jenne, R., Kitaev, L., Landwehr, J., Keeler, M., Leavesley, G., Schaake, J., Strzepek, K., Sundarvel, S.S., Takeuchi, K., Webster, F., 2001. Global water data: a newly endangered species. In: Eos Trans AGU. https://doi.org/10.1029/01EO00031.

Xu, T., Weng, B., Yan, D., Wang, K., Li, X., Bi, W., Li, M., Cheng, X., Liu, Y., 2019. Wetlands of international importance: status, threats, and future protection. IJERPH 16, 1818. https://doi.org/10.3390/ijerph16101818.